Hybrid levan–Ag/AgCl nanoparticles produced by UV-irradiation: properties, antibacterial efficiency and application in bioactive poly(vinyl alcohol) films

Anissa Haddar, [ID] *[ab] Emna Ben Ayed,[c] Assaad Sila,[ad] Jean-Luc Putaux, [ID] [e] Ali Bougatef[ab] and Sami Boufi[c]

Foodborne diseases caused by resistance of microorganisms to multiple antimicrobial agents have emerged as a major public health concern around the world. The search for potential antimicrobials has resulted in the emergence of metal nanoparticles for protection against these infections. In this study an eco-friendly and green approach was used to biosynthesize hybrid Ag/AgCl nanoparticles (NPs), using levan from *Bacillus mojavensis* as a stabilizing/reducing agent, with a high efficiency against a broad spectrum of foodborne bacteria as well as biofilm formations. The morphology and physicochemical characteristics of levan–Ag/AgCl NPs were investigated by transmission electron microscopy (TEM), X-ray diffraction (XRD), UV-vis spectroscopy (UV), dynamic light scattering (DLS) and thermogravimetric analysis (TGA). The hybrid levan–Ag/AgCl was evaluated for antibacterial activity against foodborne pathogenic bacteria (*Escherichia coli*, *Klebsiella pneumoniae*, *Salmonella enterica*, *Pseudomonas aeruginosa*, *Staphylococcus aureus*, *Micrococcus luteus*, *Listeria monocytogenes*, *Enterococcus faecalis*, *Bacillus subtilis* and *Bacillus thuringiensis*). The study demonstrated the strong efficiency of hybrid levan–Ag/AgCl NPs as a potent inhibitor against all tested strains, with much higher activity against Gram-negative than Gram-positive bacteria. Furthermore, bacterial strains were found to be highly sensitive to hybrid levan–Ag/AgCl NPs in comparison to the tested antibiotics. As a possible application of levan–Ag/AgCl NPs as an additive in packaging, PVA films with different amounts of hybrid levan–Ag/AgCl NPs were prepared by casting and their antibacterial, mechanical, and optical properties and ability to expand the shelf life of beef meat were explored. Interestingly, the amount of Ag leached out from films was below the permissible limit. This work demonstrates the strong antibacterial action of hybrid levan–Ag/AgCl NPs and their potential use in bioactive packaging material.

1. Introduction

Noble metal nanoparticles, such as silver nanoparticles (AgNPs), are one of the most investigated and used bioactive compounds. Due to their peculiar properties they have been widely used as sensors[1–3] and antimicrobial agents.[4–7] Likewise, hybrid metal/semiconductor nanocomposites have been explored and used as antibacterial agents.[8–10] Silver–silver chloride NPs (Ag/AgCl) have attracted great interest due to their remarkable photocatalytic characteristics.[11–14] Furthermore, Ag/AgCl nanoparticles showed antibacterial and antifungal activities.[15–17]

AgNPs possess a broad spectrum of action against bacteria, fungi and viruses. Due to complex mechanisms of biological interaction, they have a lower capacity to induce resistance.[18] Generally, the antimicrobial activities are correlated with the action of silver materials such as silver ions, silver NPs, silver chloride NPs, silver–silver chloride NPs or others. Ag/AgCl NPs are widely used in daily life commercial products,[19] due to their important bactericidal property coupled with low toxicity towards mammalian cells.[20,21] However, the antibacterial effect of Ag/AgCl showed some limitations due to the weak stability and aggregation tendency of the NPs.[22] Hence, increasing the Ag/AgCl NPs stability is more appropriate for important antibacterial activities.

Synthesis routes of AgNPs and Ag/AgCl NPs include physical, chemical and hybrid techniques such as photochemical,[23]

aLaboratory of Plants Improvement and Valorization of Agroressources (LAPVA), National School of Engineering of Sfax (ENIS), University of Sfax, 3038 Sfax, Tunisia. E-mail: anissa.haddar@isbs.usf.tn; Fax: +216 74 275 595; Tel: +216 74 674 354

bUniversity of Sfax, High Institute of Biotechnology, Sfax, Tunisia

cUniversity of Sfax, Faculty of Science, LMSE, BP 802, 3018 Sfax, Tunisia

dDepartment of Life Sciences, Faculty of Sciences of Gafsa, Gafsa University, 2112 Gafsa, Tunisia

eUniv. Grenoble Alpes, CNRS, CERMAV, F-38000 Grenoble, France

electrochemical,[24] and irradiation[25] procedures. The most common method was the chemical reduction to develop AgNPs with different sizes and morphologies.[26] Nevertheless, chemical reducing agents can be harmful to living organisms and result in the production of toxic byproducts. AgNPs can be produced with many defined shapes and in large amounts *via* a biologically-controlled synthesis.[27] In this green chemistry approach, sugars, like sucrose,[28] and polysaccharides, such as starch,[29] chitosan,[30,31] or cellulose[32] have been used as reducing and stabilizing agents.

Levan is a naturally occurring polymer with β-2,6-linked fructosyl units. The excellent biocompatibility, biodegradability and non-toxicity of levan makes it a valuable polymer for bio-based materials development.[33,34] Moreover, levan has been widely used in the food, cosmetic and pharmaceutical sectors as antitumor,[35] anti-inflammatory[36] and antioxidant agent.[37] Levan application has now extended into the field of nanotechnology, where it is used as capping agent for NPs synthesis.[38–42] Due to its chemical characteristics, levan can be distinguished from other biopolymers by its good solubility in oil, high water and oil holding, good biocompatibility, low viscosity and stability to heat, acid, and alkali.[43,44] Levan has been reported to form NPs by self-assembly in water.[45] The levan produced by *Acetobacter xylinum* NCIM2526 has been reported as a potential candidate for biosynthesis of Ag and Au nanoparticles.[46] Authors attribute this property of levan to the large number of hydroxyl groups in the structure that establish electrostatic interaction with the NPs, allowing their stabilization. In the same context, González-Garcinuño *et al.*[47] prepared spherical levan silver-coated nanoparticles with bactericidal effect.

Microbial contamination of foods is one of the major problems, considering the impact on the public health due to foodborne diseases.[48] Even though new antimicrobial agents have been developed, none has shown to be totally effective against multidrug-resistant bacteria and bacteria that grow on biofilms.[49] This study was undertaken to show the promising antibacterial and antibiofilm properties of Ag/AgCl nanoparticles.

Despite the existing studies on the different properties of bacterial levan and its use on the production of AgNPs, there has been no report, to our best knowledge, presenting the biosynthesis of hybrid levan–Ag/AgCl NPs. The present study, levan acted as a reducing and stabilizing agent to produce levan–Ag/AgCl NPs. The size distribution of the NPs was evaluated by transmission electron microscopy (TEM) and the crystallinity was assessed using X-ray diffraction (XRD). The antimicrobial properties of the resulting levan–Ag/AgCl NPs against Gram-positive and Gram-negative bacteria were investigated. Moreover, the development of poly(vinyl alcohol) bioactive nanocomposite films functionalized with levan–Ag/AgCl nanoparticles for meat packaging was studied.

2. Material and methods

2.1. Production and purification of levan from *B. mojavensis*

Levan was produced using a culture medium containing sucrose as the main carbon source. The composition of the medium used for the cultivations, was (in g L^{-1}): 50 sucrose; 0.4 CaCl$_2$; 1.5 K$_2$HPO$_4$; 0.2 KH$_2$PO$_4$; 0.15 MgSO$_4 \cdot$7H$_2$O and 2 yeast extract. The pH of the culture was adjusted to 7.0 before autoclaving, and the flasks were incubated in an orbital shaker at 150 rpm, at 37 °C for 48 h. After ethanol precipitation and dialysis, levan was purified by ethanol precipitation fractionation according to our previously reported data.[44]

2.2. Synthesis of hybrid levan–Ag/AgCl nanoparticles

AgNO$_3$ (12.5 mL, 0.02 M) was dissolved in distilled water and transferred into a 50 mL beaker. While the silver salt solutions were stirred, 37.5 mL of 0.5% w/v levan solution in distilled water were added and exposed to two 8W Fluorescent UV-C Tube Lights (Philips/Osram) during 10–30 min. The irradiation source was maintained at about 30 cm from the vessel containing the levan–AgNO$_3$ solution.

2.3. Characterization of synthesized hybrid levan–Ag/AgCl nanoparticles

2.3.1. Thermogravimetric analysis. The thermogravimetric analysis (TGA) was performed with a thermogravimetric analyzer (TGA 400 PerkinElmer). Samples were about 5 mg and the heating cycle was from 50 to 800 °C at a heating rate of 10 °C min^{-1} under air flow.

2.3.2. X-ray diffraction (XRD) analysis. XRD profiles were recorded with a Bruker AXS reflection diffractometer (Madison, WI, USA) using the CuKα radiation, generated at 30 kV and an incident current of 100 mA. Hybrid levan–Ag/AgCl samples were dried and cut in small pieces and the scanning was performed from 5 to 40° using 0.05° and 10 s as a scanning and time step, respectively. The crystallinity index (CrI) was calculated from the XRD patterns using Segal's method.[50]

2.3.3. Dynamic light scattering (DLS). The average diameter of hybrid levan–Ag/AgCl NPs was determined using DLS (Malvern Zetasizer Nano S, Malvern Instruments Ltd., Malvern, UK). The sample was diluted 10 times. Each measurement was repeated three times, and the average value was retained as the particle size.

2.3.4. Transmission electron microscopy (TEM). Droplets of dilute levan–Ag/AgCl suspension were deposited on freshly glow-discharged carbon-coated copper grids and allowed to dry after negative staining with 2 wt% uranyl acetate. The specimens were observed with a JEOL JEM-2100-Plus microscope operating at 200 kV and images were recorded using a Gatan Rio 16 camera. The size of the AgNPs was measured from the images using the ImageJ software.

2.4. Antibacterial and anti-biofilm activities of hybrid levan–Ag/AgCl nanoparticles

2.4.1. Bacterial strains. Gram-negative bacteria (*Escherichia coli* (ATCC 25922), *Klebsiella pneumoniae* (ATCC 13883), *Salmonella enterica* (ATCC 43972), *Pseudomonas aeruginosa* (ATCC 27853)) and Gram-positive bacteria (*Staphylococcus aureus* (ATCC 25923), *Micrococcus luteus* (ATCC 4698), *Listeria monocytogenes* (ATCC 43251), *Enterococcus faecalis* (ATCC 29212),

Bacillus subtilis (ATCC 6633), *Bacillus thuringiensis* (isolated in laboratory)) were used in this study.

2.4.2. Anti-bacterial activity of hybrid levan–Ag/AgCl nanoparticles. Culture suspensions (100 μL) of the microorganisms (10⁶ colony-forming units, CFU mL⁻¹) were inoculated onto the surface of spread on Luria–Bertani (LB) agar. Then, hybrid levan–Ag/AgCl nanoparticles at concentrations of 2.5, 5, 10, 20 and 40 μg mL⁻¹ were loaded into wells (5 mm in diameter) punched in the agar layer. Thereafter, the agar plates were kept for 1 h at 4 °C, and then, they were incubated for 24 h at 37 °C. The antimicrobial activity was evaluated by determining the zone of growth inhibition (diameter expressed in millimeters) around the wells. The growth of bacteria in liquid broth containing various concentrations of hybrid levan–Ag/AgCl NPs was investigated. Log phase bacterial cultures in LB medium were incubated at 37 °C at 150 rpm, after the addition of levan–Ag/AgCl NPs at different concentrations (2.5, 5, 10, 20 and 40 μg mL⁻¹). Control broths were used without NPs. The bacterial growth was monitored at a 2 h interval of by the absorbance of the culture media at 600 nm.

2.4.3. Determination of minimal inhibitory concentration (MIC). The MIC was defined as the lowest concentration of levan–Ag/AgCl NPs at which no visible growth of the bacterial strains was observed. It was determined using microbroth dilution method in a 96-wells microtiter culture plate as described by Andrews.[51] The bacterial strains treated with two-fold serial dilutions of hybrid levan–Ag/AgCl NPs and ranging from 2.5 to 80 μg mL⁻¹ were incubated at 37 °C for 24 h.

2.4.4. Inhibition of biofilm forming abilities of hybrid levan–Ag/AgCl nanoparticles. The inhibition of biofilm formation after treatment with levan–Ag/AgCl NPs was quantified by employing the microtiter crystal violet assay.[52] Briefly, 20 μL of freshly cultured bacteria was admixed with 180 μL of varying concentrations (2.5, 5, 10, 20, and 40 μg mL⁻¹) of hybrid levan–Ag/AgCl NPs and the plates were then kept in incubator for 24 h. The cells without levan–Ag/AgCl NPs were considered as control group. After incubation, the content from the microtiter wells was decanted and gently washed with phosphate-buffered saline (PBS) and left for drying. The adhered biofilm biomass was then stained with a crystal violet solution (0.1% w/v) for 30 min. The excess dye was decanted, washed again with PBS and the wells allowed until completely dry. The stained biofilm was then solubilized in 95% ethanol and quantified by optical density at 595 nm.[53]

2.5. Preparation of PVA nanocomposite films functionalized with hybrid levan–Ag/AgCl nanoparticles

A PVA solution (10% w/v) was prepared by dissolving PVA in distilled water under stirring for 3 h at 85 °C. Hybrid levan–Ag/AgCl NPs were added to the PVA solutions and mixed under continuous stirring at room temperature (25 °C) for at least 1 h to make sure that the mixture was completely homogeneous. Glycerol was added as a plasticizer to the hybrid levan–Ag/AgCl–PVA mixture solution up to a fraction of 5% (based on PVA weight).

The film-forming solutions were cast in a plastic mold and left at 25 ± 2 °C during 24 h until complete evaporation of water.

The resulting PVA–levan–Ag/AgCl nanocomposite films (LSNFs) were then stored in desiccators containing Mg(NO₃)₂ saturated solutions, at 25 °C for 48 h and 50% of relative humidity. LSNF1, LSNF2, and LSNF3 films were prepared by using 0.5, 1, and 2% of hybrid levan–Ag/AgCl NPs, respectively, while LSNF0 contained only PVA.

2.5.1. Mechanical properties of hybrid levan–Ag/AgCl–PVA blend films. The tensile strength (TS) and elongation at break (EAB) of the films were measured as described by Iwata *et al.*[54] using an Instron testing machine. The test was performed in a controlled environment at 25 °C and 50% relative humidity (RH). Four film samples (2 cm × 4 cm) with the initial grip length of 3 cm were used for testing. The film samples were clamped and deformed under tensile loading using a 100 N load cell with the cross-head speed of 5 mm min⁻¹ until the samples were broken. TS values were calculated by dividing the maximum load (N) by the initial cross-sectional area (m²) of the specimen. EAB was calculated as the ratio of the final length at the point of sample rupture to the initial length of the specimen and expressed as a percentage.

2.5.2. Optical absorption analysis. Nanocomposite film samples were cut into rectangles (1 cm × 3 cm) and placed in the spectrophotometer test cell. The barrier properties of films were measured at wavelengths ranging between 300 and 800 nm, using a UV-visible spectrophotometer.

2.5.3. Antibacterial activity of PVA–levan–Ag/AgCl nanocomposite films. PVA–levan–Ag/AgCl nanocomposite films were tested for their antibacterial activities using the agar well diffusion method. *E. coli* (ATCC 25922), *K. pneumoniae* (ATCC 13883), *S. enterica* (ATCC 43972) and *P. aeruginosa* (ATCC 27853) *S. aureus* (ATCC 25923), *M. luteus* (ATCC 4698), *L. monocytogenes* (ATCC 43251) and *E. faecalis* (ATCC 29212) were selected for this investigation. The bacteria were firstly cultured in a flask containing 9 mL of LB. The culture was incubated at 37 °C at 150 rpm for 18 h. Then, 100 μL aliquots of each culture suspension (10⁶ CFU mL⁻¹) were taken for antibacterial assays. The nanocomposite films (1 cm × 1 cm) were first sterilized by UV light for 10 min and then placed on the plate surface and incubated for 24 h at 37 °C for bactericidal activity assay. The antibacterial activity was assessed by the appearance of an inhibition area below or around the film. Pure PVA films were used for comparison.

2.6. Application of the active films for minced beef meat packaging

Fresh beef minced meat samples, purchased from local supermarket in Sfax (Tunisia), were prepared as 25 g square pieces under aseptic conditions. Then, the samples were wrapped with the prepared film samples (70 mm × 70 mm). In addition, the control meat sample was wrapped with pure PVA film at the same size. All beef meat samples were stored for 7 days at 4 °C and analyzed at 1, 3, 5 and 7 days.

2.7. Microbiological analyses of beef meat during storage

Microbiological analyses were performed on the whole of the minced meat. Samples of each minced meat were suspended in

sterile peptone–water solution and homogenized for 2 min at room temperature. Total aerobic counts were enumerated on Plate Count Agar (PCA), incubated at 30 °C for 48 h. Coliforms were enumerated on Violet Red Bile Lactose agar (VRBL), incubated for 24 h at 37 or 44 °C for total and fecal coliforms, respectively. Psychrophilic bacteria were evaluated using PCA after incubation at 4 °C for 5 days. *Salmonella* was detected by a presence–absence test. First, 25 g of samples were homogenized in 225 mL of buffered peptone water and incubated for 24 h at 37 °C. After incubation, 1 mL was transferred to 10 mL of selenite–cystine broth and incubated at 37 °C for 24 h. Then, a loop full of broth was plated onto Hektoen medium and incubated at 37 °C for 24 h.

2.8. ICP-OES analysis of released silver

Composite films (10 cm × 10 cm) containing hybrid levan–Ag/AgCl NPs were left in 1 L of 3% (w/w) acetic solution for 5 days at 40 °C under shaking and the total Ag content was evaluated by inductively coupled plasma optical emission spectrometer (PerkinElmer Optima7300 DV ICP-OE) after acidifying with nitric acid. For calibration, a silver standard solution was used. The limit of detection for the ICP-AES was taken as 0.005 mg L^{-1}.

3. Results and discussion

3.1. Levan–Ag/AgCl nanoparticle synthesis and morphological characterization

Levan was isolated from the *B. mojavensis* culture, and its backbone was identified as main composed of D-fructosyl residues linked by β-2,6-glycosidic bonds that can be occasionally branched through β-2,1-linkages.[44] The hybrid levan–Ag/AgCl material was prepared by simply adding AgNO$_3$ aqueous solution to levan, then exposed to UV-light irradiation from 10 to 30 min. The suspension progressively turned to yellow-brown indicating the generation of hybrid levan–Ag/AgCl NPs (Fig. 1A). This hypothesis was confirmed through multiple characterization methods. The UV-Vis spectrum showed a broad absorption band peaking at 420–430 nm which is typical of plasmon resonance band for hybrid levan–Ag/AgCl NPs (Fig. 1B). The increasing intensity of this band with time indicates an increase of the concentration of hybrid levan–Ag/AgCl with irradiation time (Fig. 1B). The broadening of the plasmon band is likely due to the growth of hybrid levan–Ag/AgCl NPs. Another direct evidence of the generation of metallic Ag/AgCl was provided by the XRD profile from freeze-dried hybrid levan–Ag/AgCl NPs (Fig. 1C), where the characteristic peaks of metallic Ag located at 37.5 and 43.5°
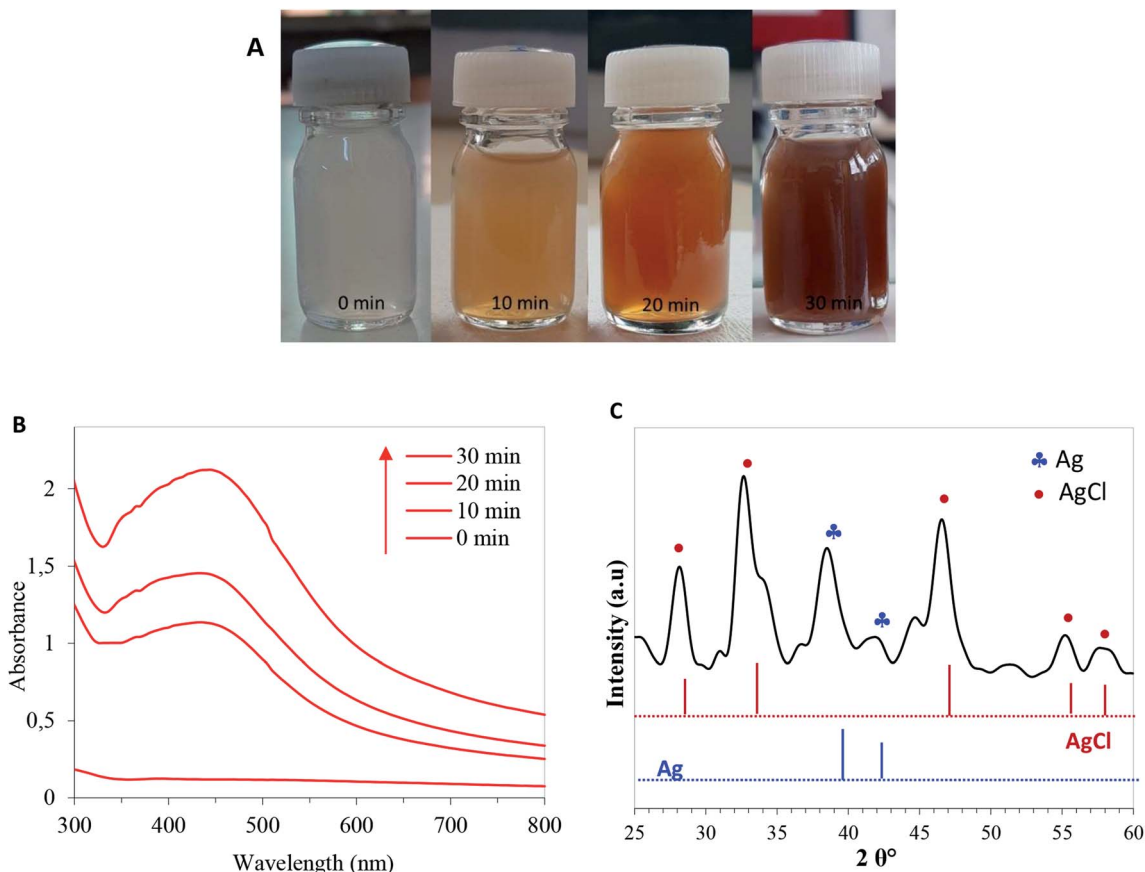

Fig. 1 (A) Photos of the levan–AgNO3 solution at different irradiation time, (B) time-evolution of the UV–Vis absorption of levan solution after addition of AgNO3 solution and exposition to UV-light, (C) XRD patterns of levan–AgNO3 after exposition to UV-light during 30 min and lyophilization.
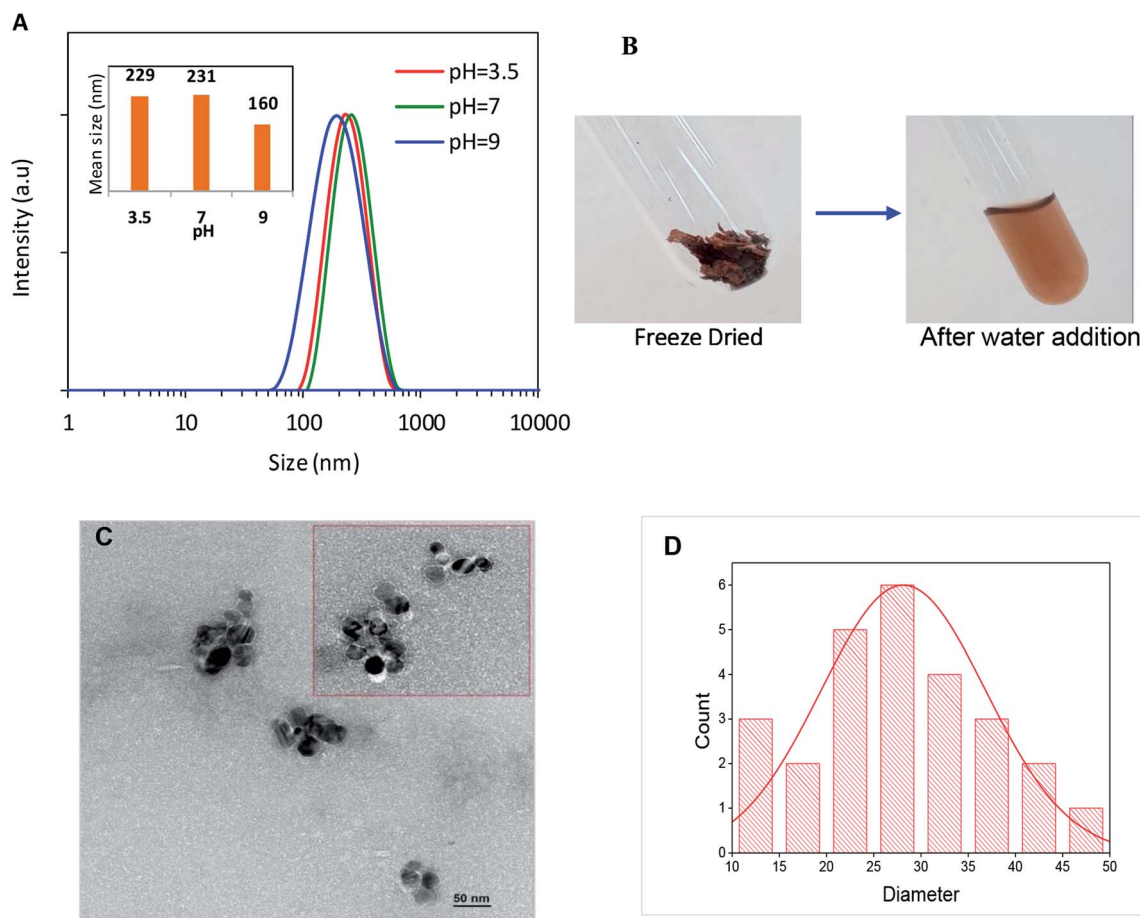
Fig. 2 (A) Particle size distribution of hybrid levan–Ag/AgCl suspension at different pH, measured by DLS, and (B) freeze-dried levan–Ag/AgCl after addition of water; (C) TEM image of hybrid levan–Ag/AgCl NPs obtained under 0.5% (w/w) levan solution containing AgNO3 (5×10^{-3} M) exposed to UV-light during 30 min; (D) size distribution histogram of the nanoparticles measured from the TEM images.
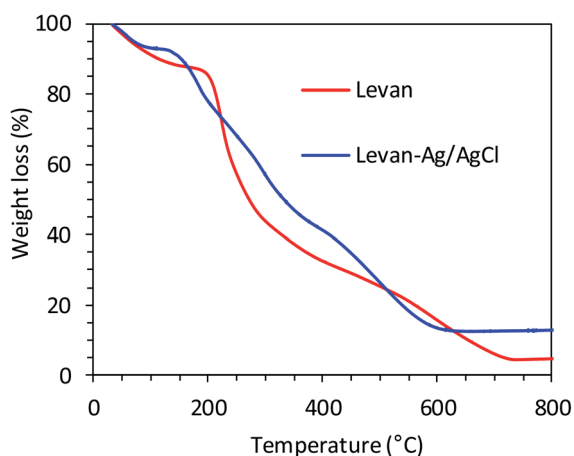

Fig. 3 TGA of levan and hybrid levan–Ag/AgCl under air atmosphere.

corresponding to (1 1 1) and (0 0 2) reticular planes of cubic Ag (JCPDS no. 65-2871). However, in addition to Ag peaks, the spectra showed intense peaks at 27.8, 32.6, 46.4, 54.9 and 57.6° which are characteristic of (1 1 1), (2 0 0), (2 2 0), (3 1 1) and (2 2 2) diffracting planes of cubic AgCl crystals (JCPDS no. 31-1238).

This means that AgCl was also formed in addition to Ag, the presence of which is probably due to the existence of residual Cl⁻ ions introduced during the synthesis of levan.

The average particle size of hybrid levan–Ag/AgCl at different pH, assessed by DLS, revealed a monomodal distribution in size peaking at around 230 nm at a pH from 3.5 to 7 and decreasing to about 160 nm at pH 9 (Fig. 2A). The zeta potential remained roughly unchanged at around −7 to −9 mV, suggesting that the particles of hybrid levan–Ag/AgCl were barely charged and that the colloidal stability was ensured by steric effect, presumably by the polyfructose chains encapsulation the hybrid levan–Ag/AgCl NPs. The high density of hydroxyl groups in levan (3 groups/fructosyl unit) along with the branching structure are likely to contribute to the capping of the Ag/AgCl NPs generated by the levan chains. The absence of charged groups such as carboxyl, sulfate or amine justifies the low magnitude of zeta-potential of hybrid levan–Ag/AgCl. Interestingly, hybrid levan–Ag/AgCl NPs could be easily redispersed by gentle shaking after lyophilization (Fig. 2B), which contributes to facilitate the use of hybrid levan–Ag/AgCl NPs as additive in waterborne materials. TEM images of a dry specimen revealed the presence of spherical levan–Ag/AgCl NPs with a size ranging from 20 to 50 nm

Table 1 Zone of inhibition (mm) and MIC ($\mu g\ mL^{-1}$) for Gram-positive and Gram-negative bacterial strains in the presence of different levan–Ag/AgCl NPs concentrations. Control: Ampicillin (30 $\mu g\ mL^{-1}$ for all tested bacteria); NH: No inhibition

	Control	Levan–Ag/AgCl PNs (μg)/zone of inhibition (mm)					MIC (μg)
Bacterial strains	30	2.5	5	10	20	40	Levan–AgPNs
Gram-positive bacteria							
S. aureus	NH	9 ± 0.51	11 ± 0.75	22 ± 0.58	24 ± 0.26	28 ± 0.99	40
L. monocytogenes	33 ± 1.1	13 ± 0.23	17 ± 0.63	18 ± 0.44	20 ± 0.43	25 ± 0.81	40
M. leteus	35 ± 0.82	18 ± 0.55	22 ± 0.91	25 ± 0.39	27 ± 096	29 ± 0.66	40
E. fecalis	35 ± 0.95	21 ± 0.368	25 ± 0.87	25 ± 0.73	27 ± 0.70	27 ± 0.83	20
B. subtilis	31 ± 0.88	22 ± 0.50	24 ± 0.64	25 ± 0.48	27 ± 0.53	26 ± 0.66	40
B. thuringiensis	30 ± 0.73	21 ± 0.37	24 ± 0.29	25 ± 0.41	28 ± 0.70	26 ± 0.74	40
Gram-negative bacteria							
E. coli	34 ± 1.0	17 ± 0.40	22 ± 0.60	24 ± 0.97	25 ± 0.69	32 ± 0.86	20
P. aeruginosa	NH	12 ± 0.33	19 ± 0.42	22 ± 0.58	24 ± 0.31	31 ± 0.53	20
S. typhimurium	32 ± 0.71	13 ± 0.28	19 ± 0.38	22 ± 0.84	24 ± 0.36	32 ± 0.77	40
K. pneumoniae	34 ± 0.85	12 ± 0.54	13 ± 0.27	20 ± 0.37	22 ± 0.42	30 ± 0.94	20

which were smaller comparing to the particle size distribution obtained from DLS (Fig. 2A). The higher size given from DLS suggested that some aggregation occurred among the generated hybrid levan–Ag/AgCl NPs, which was confirmed by TEM images (Fig. 2C). In fact, given the lack of ionic charges on the surface of levan–Ag/AgCl NPs, weak aggregation of the elementary particles is inevitable leading to the formation of coarse particles with size from 100 to 400 nm (Fig. 2A). However, we infer that the presence of levan encapsulating the Ag/AgCl NPs contributed to avoid the irreversible aggregation thanks to its hydration with water molecules and gentle shaking redisperse again the particles. This is attested by the facile redispersion of lyophilized levan–Ag/AgCl after addition of water (Fig. 2B). The hypothesis of encapsulation of Ag/AgCl by levan is supported by TEM observation, where the particles seem to be coated by an organic layer (Fig. 2C inset).

The TGA thermogram of neat levan and hybrid levan–Ag/AgCl NPs under air atmosphere (Fig. 3), showed a first weight loss from 50 to 150 °C corresponding to the evaporation of water bound to levan. Immediately after this event, an important weight loss of about 40–50% extending from 190 to 240 °C was observed, which is due to the thermal decomposition of levan involving the breaking of the branch chain linkages β-(2,1) and the main chain β-(2,6) backbone.[55]

In levan–Ag/AgCl NPs, the thermal decomposition was observed at lower temperature than levan, starting at about 170 °C and involving three steps at 170–250, 250–350 and 350–650 °C. The ash content increased from about 4.5% for neat levan to 12% for levan–Ag/AgCl NPs, meaning that the content in Ag/AgCl in levan–Ag/AgCl NPs may be estimated to about 7.5%. Although numerous papers have reported the successful use of carbohydrates and biopolymers such as cellulose, chitosan, pectin, guar gum, inulin and levan as reducing and stabilizing agent to generate stable hybrid levan–Ag/AgCl NPs, the exact mechanism explaining the generation, the growth and the stabilizing action of these biopolymers has not been fully elucidated yet. However, it was suggested that hydroxyl groups are on the reducing species and will act in a similar way like

polyethylene glycol.[28,29,56,57] In the present case, we assumed that the formation of AgCl was the first step occurring immediately following the addition of AgNO₃ solution, thanks to the presence of chloride ions in the levan solution. Upon absorption of a photon, AgCl produces one electron and one hole, followed by electron transfer to transform the Ag⁺ to an Ag atom to generate Ag cluster by repeating this process. This phenomenon is similar to that occurring in black and white photography,[58] where silver halides were photoreduced to Ag, forming the image, when exposed to light.

3.2. Antibacterial activity of hybrid levan–Ag/AgCl NPs

To investigate the antibacterial action of the hybrid levan–Ag/AgCl, ten pathogenic bacteria, four Gram-negative: *E. coli*, *K. pneumoniae*, *P. aeruginosa*, *S. enterica* and six Gram-positive: *S. aureus*, *M. luteus*, *L. monocytogenes*, *E. faecalis*, *B. subtilis* and *B. thuringiensis* were tested using the agar well diffusion method (2.5, 5, 10, 20 and 40 $\mu g\ mL^{-1}$). The control was bacteria grown without levan–Ag/AgCl NP addition. The zone inhibition values of tested bacteria and ampicillin used as control are given in Table 1. Levan–Ag/AgCl NPs exhibited a concentration-dependent growth inhibition efficacy against both Gram-positive and Gram-negative bacteria. It was found that the antibacterial effect of levan–Ag/AgCl NPs were not uniform across studied foodborne pathogenic strains. Results showed also that *S. aureus* and *P. aeruginosa* were completely resistant to ampicillin, but all tested strains were sensitive to levan–Ag/AgCl NPs at all concentrations. The mean value of zones of inhibition noted for foodborne pathogenic bacteria were in the range of 25 to 32 mm. Similar results were obtained with *S. aureus* and *E. coli* in the presence of 0–12 $\mu g\ mL^{-1}$ of AgNPs synthesis with levan produced by *B. amyloliquefaciens* PB6.[59] In the same context, González-Garcinuño[47] reported a significant bactericidal effect of silver nanoparticles produced using levan synthesis in a cell free system. Additionally, silver nanoparticles prepared using carbohydrates (sucrose, soluble and waxy corn starch) as reducing and stabilizing agents exhibited excellent bactericidal activity against both Gram-positive and Gram-

negative bacteria.[25] The results indicated that levan–Ag/AgCl NPs were more effective against Gram-negative than Gram-positive bacteria. This difference agrees with the report by González-Garcinuño,[47] Kawahara,[60] and Taglietti.[61] The authors attributed this difference to the structure between the cell wall the two groups of bacteria. In fact, it can be associated with the penetration of the *B. mojavensis* levan into the cytoplasm of the bacteria, with the subsequent local interaction of Ag with cell components causing the destruction of the cells.

Table 1 shows that the minimum inhibitory concentration (MIC) of hybrid levan–Ag/AgCl NPs is within the 20–40 $\mu g\ mL^{-1}$ range. Moreover, the tested hybrid levan–Ag/AgCl NPs showed a low efficiency against Gram-positive bacteria except for *E. fecalis*, but a high inhibitory capacity against Gram-negative bacteria. This is probably due to the immobilization of silver ions to the levan and formation of (Ag, AgCl) NPs/levan complex, which subsequently causes the inhibitory activity. The MIC of levan–Ag/AgCl NPs was lower compared to that of Ag/AgCl synthesized using an aqueous plant extract (0.25–1 $mg\ mL^{-1}$).[62] In the same context, Zhao[63] reported a MIC of Ag/AgCl/anhydrous basic bismuth nitrate (ABBN) against *E. coli* of about 35 $\mu g\ mL^{-1}$.

The extent of bactericidal activity of *B. mojavensis* levan–Ag/AgCl can be assessed by studying the growth kinetics of bacterial strains in dose-dependent manner. Growth kinetics in liquid media of all tested foodborne pathogenic bacteria at different concentrations of levan–Ag/AgCl NPs are shown in Fig. 4. Successful antibacterial efficacy of levan–Ag/AgCl NPs was observed. The incorporation of levan–Ag/AgCl NPs affected the growth kinetics as compared to the control (growth without levan–Ag/AgCl NPs). The partial growth of bacterial strains was visible up to 5 $\mu g\ mL^{-1}$ dose of levan–Ag/AgCl NPs. These results confirmed the positive impact of levan–Ag/AgCl NPs in the inhibition of pathogenic bacteria. Similar to this study, Zhang[59] investigated the effect of AgNPs capped with *B. amyloliquefaciens* PB6 levan against *S. aureus* and *E. coli* in liquid media. The authors reported a positive effect of AgNPs against the studied strains.

In support of the above discussions, the antibacterial effect of levan–Ag/AgCl NPs was further investigated using information from the MIC assay on solid media. *E. coli, K. pneumoniae, S. enterica, P. aeruginosa, S. aureus, M. luteus, L. monocytogenes, E. faecalis, B. subtilis* and *B. thuringiensis* were used at concentrations ranging from 2.5 $\mu g\ mL^{-1}$ to 80 $\mu g\ mL^{-1}$. Fig. 5A depicts the effective antibacterial activity at various levan–Ag/AgCl NP concentrations. Beyond 40 $\mu g\ mL^{-1}$, there was no bacterial growth for all tested foodborne strains. The CFU of foodborne pathogenic bacteria was determined after incubation at 20 h (Fig. 5B). The results showed that levan–Ag/AgCl NPs inhibited bacterial growth of *E. coli, P. aeruginosa, K. pneumoniae, E. faecalis* at 20 $\mu g\ mL^{-1}$. Moreover, *S. enterica, S. aureus, M. luteus, L. monocytogenes, B. subtilis* and *B. thuringiensis* were inhibited at 40 $\mu g\ mL^{-1}$. This finding confirms previous results on the antibacterial activity in liquid media. However, the mechanisms of action of AgNPs on the bacterial growth is still a matter of debate. The generation of reactive oxygen species (ROS) likely causes structural and morphological damages of the microorganisms.[64] Some authors suggested that probably the release of silver ion by the silver nanoparticles into bacteria

can cause cell lysis or inhibit cell transduction and bacterial death.[65,66]

3.3. Influence of levan–Ag/AgCl on antibiofilm activity

Levan–Ag/AgCl NPs were also tested against foodborne pathogenic producing biofilm bacteria. The results showed that levan–Ag/AgCl NPs exhibited inhibitory activity with varying efficiencies, depending on the used concentrations. The capacity of levan–Ag/AgCl NPs to inhibit the biofilm formation increased proportionally with their concentrations (2.5, 5, 10, 20 and 40 $\mu g\ mL^{-1}$) (Fig. 6). At a concentration of 40 $\mu g\ mL^{-1}$,
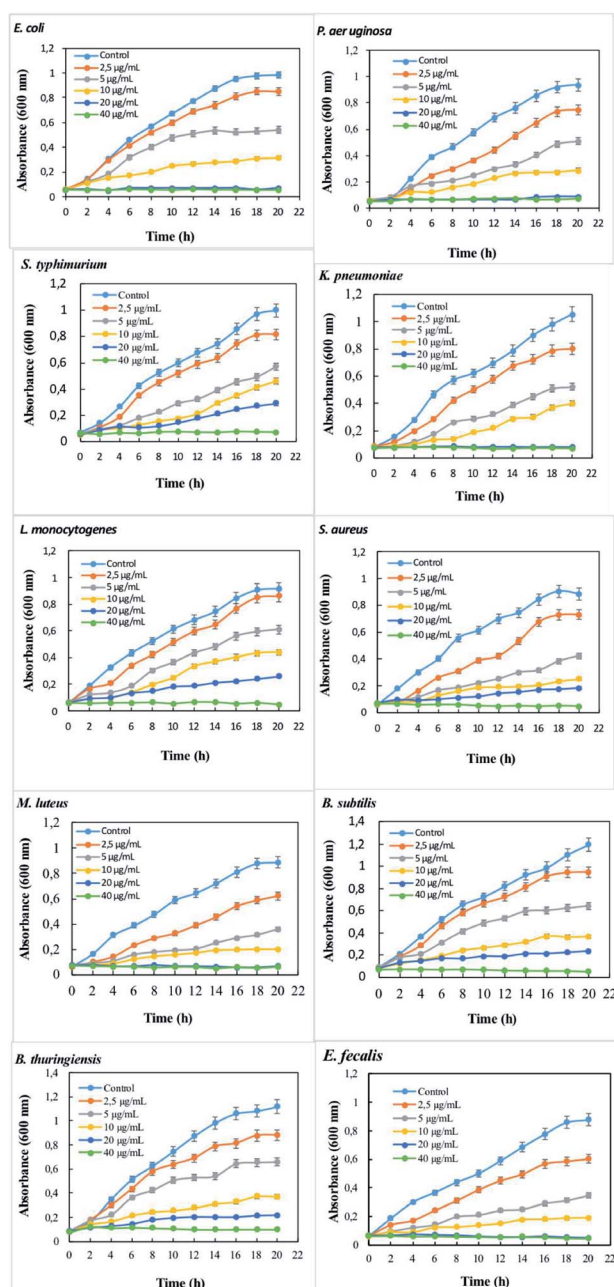

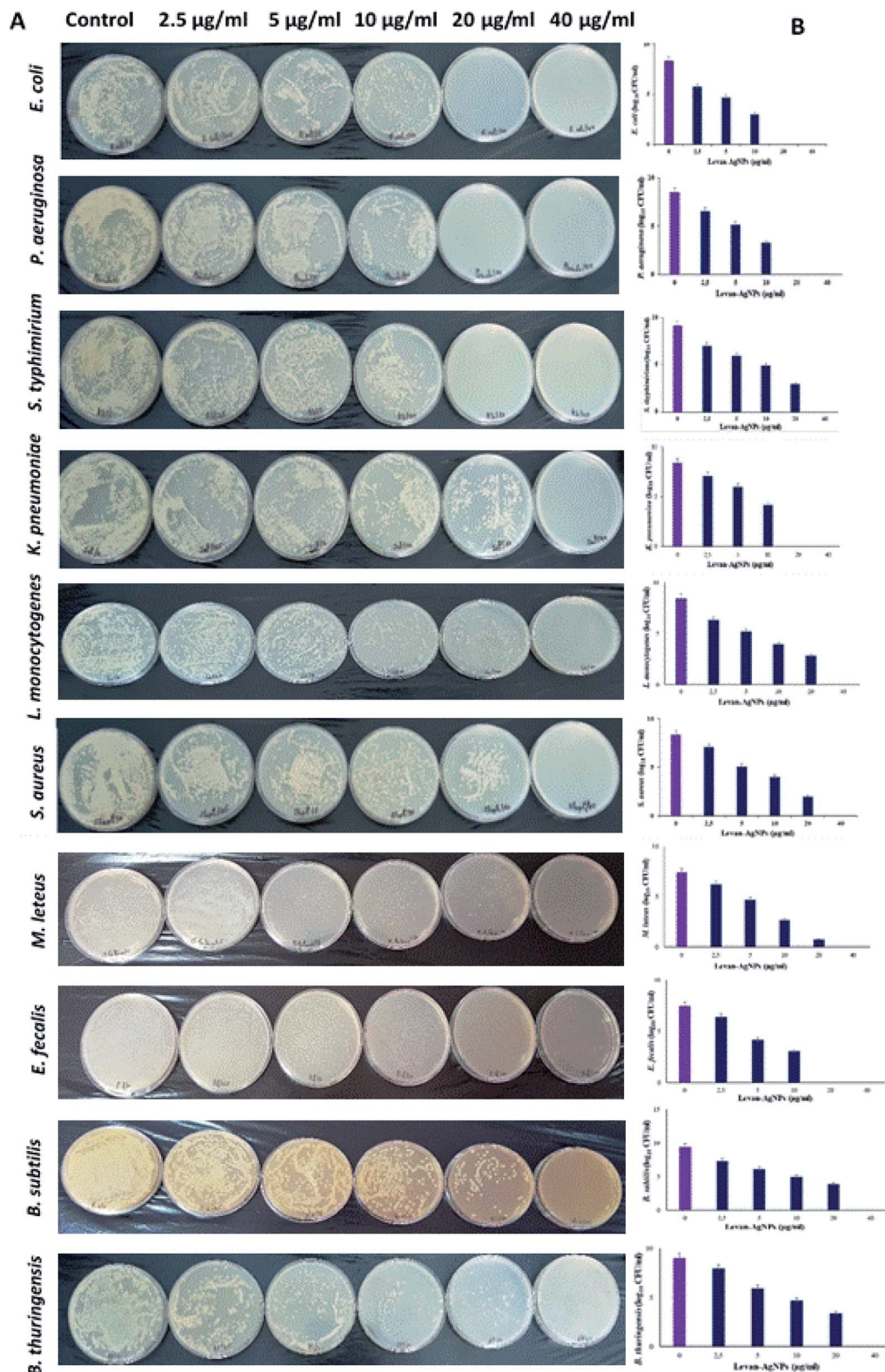Fig. 4 Dose-dependent antimicrobial efficacy of levan–Ag/AgCl NPs against Gram-negative and Gram-positive bacteria.

Fig. 5 (A) The antibacterial activity was tested against foodborne pathogenic bacteria on solid media. (B) The noted log10 CFU mL^{-1} readings from three biological replicates are plotted in Y-axis against different concentrations of levan–Ag/AgCl tested at X-axis, are shown as bar graphs.

levan–Ag/AgCl NPs inhibited Gram-negative bacteria: *P. aeruginosa*, *K. pneumoniae*, *E. coli*, and *S. typhimurium* by 91.65, 89.2, 92.5, and 89.8% of biofilm inhibition, respectively. The

maximum percent of biofilm inhibition for Gram-positive bacteria was obtained for *B. subtilis* and *M. luteus* (93%) at 40 µg mL^{-1} followed by *S. aureus* (92.7%), *E. fecalis* and *B.*
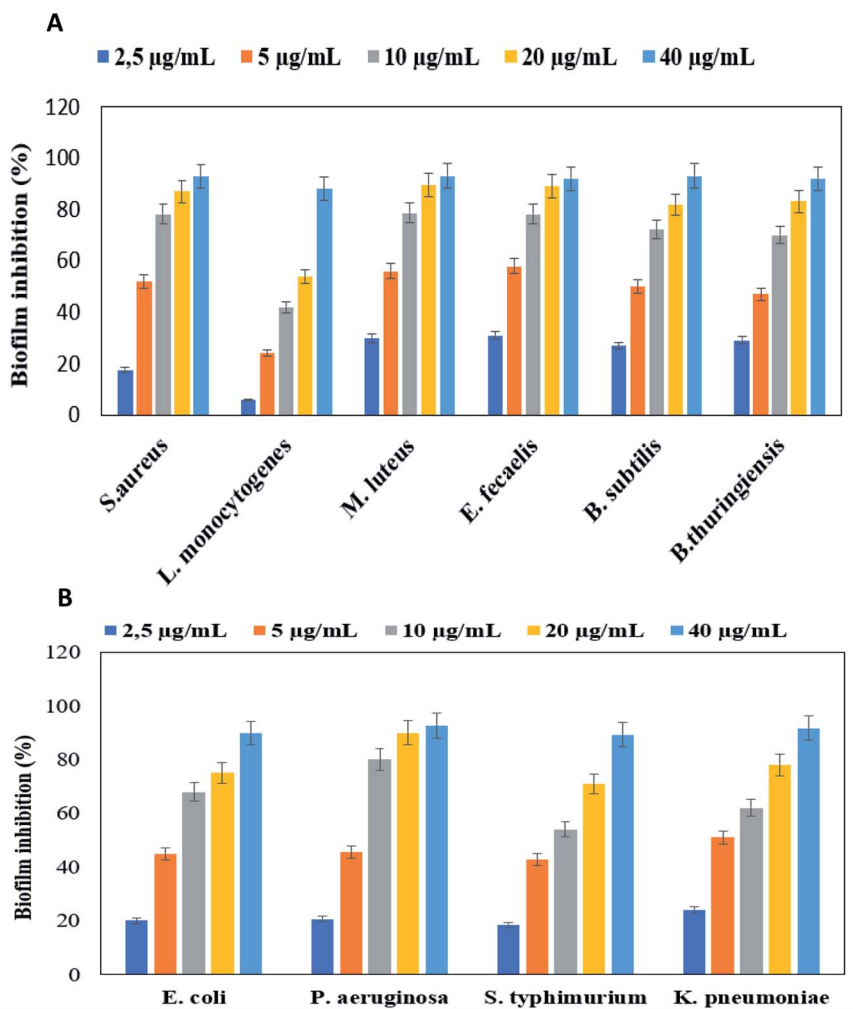
Fig. 6 Anti-biofilm activity of levan Ag/AgCl NPs against Gram-positive (A) and Gram-negative (B) bacteria.

thuringiensis (92%) and *L. monocytogenes* (88%). Interestingly, our findings showed that levan–Ag/AgCl NPs effectively inhibited biofilm of Gram-positive and Gram-negative bacteria in 24 h. In the same context, Kumar and Sujitha,[67] reported that silver glyconanoparticles using kocuran, a biopolymer produced by *Kocuria rosea*, had antibiofilm activity against *S. aureus* and *E. coli* in a concentration-dependent manner. Gum Arabic was also used as capped agent for silver nanoparticles synthesis by Ansari.[68] In their study, the authors showed an efficient activity against biofilm forming *P. aeruginosa*. Biofilm inhibition of levan–Ag/AgCl NPs may be due to the inhibitory capacity on gene expressions linked to motility and biofilm generation.[21,69] From the obtained results, it can be concluded that levan–Ag/AgCl possesses a capacity to reduce biofilm and contrast its formation.

3.4. Development and characterization of PVA films incorporating levan–Ag/AgCl nanoparticles

3.4.1. Characterization and mechanical properties of PVA–levan–Ag/AgCl films. Given the strong antibacterial action of levan–Ag/AgCl for wide ranges of bacteria, PVA films containing different amount (between 0.5 and 2% based on PVA) of levan–Ag/AgCl NPs were prepared by mixing aqueous solution of PVA and levan–Ag/AgCl NPs suspension followed by solvent casting. After complete water evaporation, transparent film was obtained and their antibacterial and aptitude to improved packaging of beef meat were investigated. The choice of fully hydrolyzed PVA polymer was justified by the wide application of PVA in packaging thanks to its high barrier property against gases (especially oxygen transmission rate (OTR)), and the possibility to dissolve PVA in hot water, making easy the preparation of the PVA–levan–Ag/AgCl films, favoring their use in food packaging.[70] The objective was to investigate how the inclusion of a small amount of levan–Ag/AgCl NPs in PVA films may introduce additional functionality to the PVA film, more specifically with regard to antibacterial properties and food conservation action. Films with three amounts of levan–Ag/AgCl NPs (0.5, 1 and 2% with respect to PVA) were prepared and tested in addition to PVA neat film. The photos of the films with different levan–Ag/AgCl NPs contents are shown in Fig. 7A. As revealed from photos of PVA–levan–Ag/AgCl films and from transmittance measurement, the inclusion of levan–Ag/AgCl

NPs at content lower than 2% did not meaningfully affect the transparency of the film.

The transmittance at 700 nm decreased from about 87% for the neat PVA film to about 81% in PVA film containing 2% levan–Ag/AgCl NPs, which is low and indicative of effective dispersion of levan–Ag/AgCl within the PVA matrix (Fig. 7B). Interestingly, it can be seen that the transmittance of PVA films incorporated with levan–Ag/AgCl NPs showed low light transmission, indicating strong absorption of light in the UV-domain in PVA–levan–Ag/AgCl films. These peculiar UV barrier properties would be beneficial in packaging application by delaying the oxidation of lipids.

The mechanical property of the PVA films at different concentrations of levan–Ag/AgCl NPs was assessed by tensile test analysis. The results shown in Fig. 7C, revealed an enhancement in the tensile strength (σ) of the films with inclusion of levan–Ag/AgCl NPs. The increment in σ with respect to the neat matrix was around 10%, 28% and 60% at levan–Ag/AgCl NP contents of 0.5, 1 and 2 wt%, respectively. This result was unexpected and suggested a possible interaction between the levan–Ag/AgCl NPs and the PVA matrix that explains the beneficial effect in the mechanical properties of the film. More work is needed to understand the mechanism by which levan–Ag/AgCl NPs affected the mechanical properties of PVA films.

3.4.2. Antibacterial activity of PVA–levan–Ag/AgCl nanocomposite films. PVA–levan–Ag/AgCl nanocomposite films efficiency on bacterial growth inhibition was investigated. Our findings revealed that Gram-positive and Gram-negative bacteria were inhibited by PVA–levan–Ag/AgCl nanocomposite films as depicted on agar well diffusion method in Fig. 8. Noticeable inhibition zones appeared for three bacteria *E. coli*, *K. pneumoniae* and *S. typhimurium* exhibiting the effective antibacterial activities of the prepared nanocomposite films and inhibition was correlated with levan–Ag/AgCl NPs concentrations. Results showed also that the diameter of inhibition zone increased with increase of levan–Ag/AgCl nanoparticles. However, PVA did not show any antibacterial effect against all foodborne pathogenic bacterial strains. Results agree with Hajji[71] who reported antibacterial activity of nanocomposite films based on chitosan–poly(vinyl alcohol) and silver nanoparticles. In another report, Xin[72] described the antibacterial capacity of chitosan/curcumin nanoparticles based zein and potato starch composite films. In the same context, Sganzerla[73] investigated the antibacterial activity of nanocomposite poly(ethylene oxide) films functionalized with silver nanoparticles and they reported a strong antibacterial efficiency of prepared films. Li and Ding,[74] reported that the silver nanoparticles may first cause the destruction of the bacterial cell membrane and can also damage some phosphate lipids and proteins and induce cell death. PVA nanocomposite film blended with 2% levan–Ag/AgCl NPs possessed the best antibacterial activity, suggesting this film could be potentially used in food application for development of packaging material.

3.5. Utilization of PVA–levan–Ag/AgCl nanocomposite films for meat packaging

Microbial contamination of meat products is found mostly on the product surface. Hence, the use of antimicrobial packaging
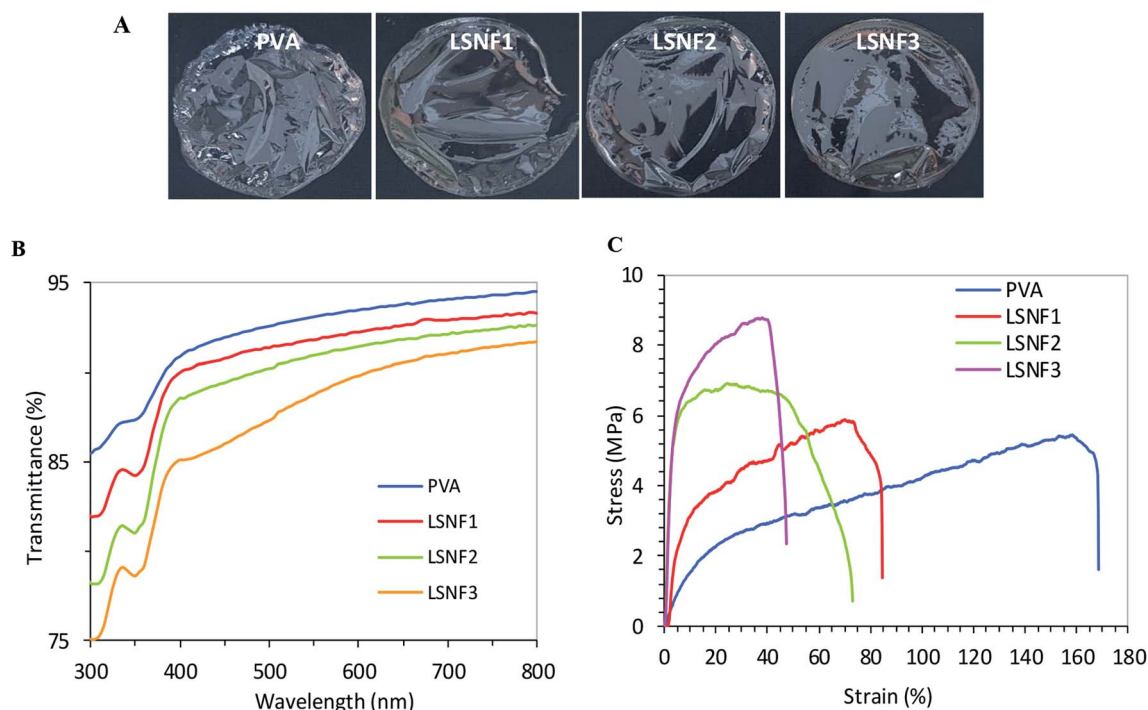

Fig. 7 (A) Photos of PVA–levan–Ag/AgCl films, (B) transmittance from 300 to 800 nm and (C) stress–strain curves of PVA films with different content in levan–Ag/AgCl. PVA: without levan–Ag/AgCl NPs, LSNF1: PVA + 0.5% levan–Ag/AgCl NPs, LSNF2: PVA + 1% levan–Ag/AgCl NPs, LSNF3: PVA + 2% levan–Ag/AgCl NPs.

Fig. 8 The digital photographs of antibacterial activities of PVA/levan–Ag/AgCl NPs nanocomposite films against Gram-positive and Gram-negative bacteria. PVA without levan–Ag/AgCl NPs, LSNF1: PVA + 0.5% levan–Ag/AgCl NPs, LSNF2: PVA + 1% levan–Ag/AgCl NPs, LSNF3: PVA + 2% levan–Ag/AgCl NPs.

would be a better alternative solution than incorporating the antimicrobial agents into the food products[75] as the packaging material interact actively with the food product and the environment.[76] Current progresses in nanotechnologies offer novel antimicrobial packaging materials with an extended shelf-life and improved safety of meat and meat products.[77]

Table 2 shows the changes of total viable counts, psychrophilic bacteria, total and fecal coliforms, and salmonella of minced beef meat packaged with pure PVA film and PVA films blend supplemented with different concentrations of levan–Ag/AgCl NPs during refrigerated storage. PVA nanocomposite films

incorporated with levan–Ag/AgCl nanoparticles exhibited significant inhibitory effects ($p < 0.05$) against tested bacteria than the control film (pure PVA without levan–Ag/AgCl NPs). Comparisons of the bacterial count reductions among the LSNFs at different concentrations of levan–Ag/AgCl NPs were significantly different ($p < 0.05$). This suggests that the highest loading concentration (2%) is more efficient to inhibit the growth of bacteria. Furthermore, it is worth mentioning that all bacterial strains were increased, except fecal coliforms, indicators of fecal contamination, were diminished for meat sample wrapped with LSNF3 over 7 days of storage. Coliforms are

Table 2 The mean microbial count (log CFU g^{-1}) of ground meat covered in PVA/levan–Ag/AgCl NPs nanocomposite films stored at 4C for 7 days[a]

Microbes	Treatment/films	Storage time (day)			
		1	3	5	7
Total viable counts (log CFU g^{-1})	PVA	4.95 ± 0.10	5.69 ± 0.15	6.02 ± 0.17	6.47 ± 0.10
	LSNAF1	4.90 ± 0.05	5.17 ± 0.11	5.90 ± 0.13	6.17 ± 0.05
	LSNAF2	4.87 ± 0.11	5.04 ± 0.12	5.60 ± 0.15	5.84 ± 0.10
	LSNAF3	4.77 ± 0.02	4.92 ± 0.09	4.98 ± 0.08	5.18 ± 0.16
Psychrophilic bacteria (log CFU g^{-1})	PVA	Absence	Absence	Absence	3.33 ± 0.11
	LSNAF1	Absence	Absence	Absence	3.00 ± 0.05
	LSNAF2	Absence	Absence	Absence	2.77 ± 0.10
	LSNAF3	Absence	Absence	Absence	2.30 ± 0.08
Total coliform (log CFU g^{-1})	PVA	3.84 ± 0.04	4.30 ± 0.11	4.55 ± 0.06	4.90 ± 0.13
	LSNAF1	3.81 ± 0.10	4.13 ± 0.15	4.23 ± 0.16	4.70 ± 0.20
	LSNAF2	3.77 ± 0.12	3.83 ± 0.09	4.00 ± 0.13	4.52 ± 0.17
	LSNAF3	3.66 ± 0.15	3.74 ± 0.16	3.85 ± 0.11	3.91 ± 0.05
Fecal coliform (log UFC g^{-1})	PVA	3.60 ± 0.06	3.71 ± 0.12	3.90 ± 0.09	4.05 ± 0.15
	LSNAF1	3.34 ± 0.11	3.40 ± 0.08	3.65 ± 0.05	3.92 ± 0.02
	LSNAF2	3.30 ± 0.15	3.32 ± 0.13	3.55 ± 0.10	3.60 ± 0.05
	LSNAF3	3.23 ± 0.08	3.17 ± 0.05	2.95 ± 0.14	2.80 ± 0.20
Salmonella	PVA	Absence	Absence	Absence	Absence
	LSNAF1	Absence	Absence	Absence	Absence
	LSNAF2	Absence	Absence	Absence	Absence
	LSNAF3	Absence	Absence	Absence	Absence

[a] PVA without levan–Ag/AgCl NPs, LSNF1: PVA + 0.5% levan–Ag/AgCl NPs, LSNF2: PVA + 1% levan–Ag/AgCl NPs, LSNF3: PVA + 2% levan–Ag/AgCl NPs.

commonly presented in nature and they are now considered sanitary indicators and food hygiene.[78]

Also, it should be noted that meat wrapped with only PVA exhibited the highest bacterial growth for all treatments in comparison with PVA blended films. The antimicrobial activity of levan–Ag/AgCl NPs is likely due to the slow release of silver ions and their interaction with the negatively charged biomolecules causing cell wall damage, structural changes in protein and its biological function and ultimately to cell death.[79] The possible oxidative damage of proteins and DNA in the microbial after interaction with Ag/AgCl NPs on the surface of PVA film may also contributed to the deactivation process as highlighted in the literature data.[80,81]

3.6. Release of Ag from nanocomposite films

For packaging films containing Ag/AgCl NPs, the possible release of silver from food contact materials by dissolution or leaching out of AgCl is inevitable, making necessary to estimate the amount of silver migration from the film. For this purpose, PVA film containing 1% levan–Ag/AgCl was immersed in 3% (w/w) acetic acid solution serving as food simulant, and the amount of released Ag after 5 days was assessed by ICP. It was found that the amount of released Ag was lower than 0.03 mg L^{-1} which fit with the European Food Safety Authority,[82] setting a migration limit of 0.05 mg L^{-1}. Two possible reasons might explain the low migration/release of Ag from PVA–levan–Ag/AgCl: the first one is the low solubility of AgCl (solubility product, K_{sp}, for AgCl in water is 1.77×10^{-10} at 25 °C), limiting the dissolution of Ag ions in water, and the second reason would be the effective binding of Ag/AgCl to levan and PVA matrix. The low migration/diffusion of Ag from PVA–levan–Ag/AgCl is of great benefice for application of levan–Ag/AgCl NPs as additive in food packaging based on fully hydrolyzed PVA films.

4. Conclusion

Employing an eco-friendly approach using levan from *B. mojavensis* as stabilizing agents gives a new viewpoint for effective levan–Ag/AgCl NPs as antibacterial agent for the development of bioactive food packaging materials. In the present study, hybrid levan–Ag/AgCl NPs were synthesized by UV-irradiation and their morphological and physicochemical characteristics were studied. Levan–Ag/AgCl showed significant antibacterial properties and antibiofilm activity against ten foodborne pathogenic bacteria. Levan–Ag/AgCl NPs incorporated in a PVA matrix showed a homogeneous morphology, with no formation of aggregates. Moreover, PVA–levan–Ag/AgCl films exhibited antibacterial activity. The antibacterial effect was directly proportional to the concentration of the Ag/AgCl NPs. Furthermore, the incorporation of PVA–levan–Ag/AgCl in nanocomposite films showed promising inhibition of bacterial growth for packaging of beef meat which can help to extend the food shelf life. These results suggest that these nanocomposite films could be effective in food packaging technology.

Conflicts of interest

There are no conflicts to declare.

Acknowledgements

References

1 S. Bothra, J. N. Solanki, S. K. Sahoo and J. F. Callan, *RSC Adv.*, 2014, **4**, 1341–1346.
2 S. Bothra, R. Kumar, R. K. Pati, A. Kuwar, H.-J. Choi and S. K. Sahoo, *Spectrochim. Acta, Part A*, 2015, **149**, 122–126.
3 S. Bothra, J. N. Solanki and S. K. Sahoo, *Sens. Actuators, B*, 2013, **188**, 937–943.
4 H. Vidya, K. Swamy and M. Schell, *J. Mol. Liq.*, 2016, **214**, 298–305.
5 Z. M. Mahdieh, S. Shekarriz, F. A. Taromi and M. Montazer, *Cellulose*, 2018, **25**, 2355–2366.
6 S. K. Srikar, D. D. Giri, D. B. Pal, P. K. Mishra and S. N. Upadhyay, *Green Sustainable Chem.*, 2016, **6**, 34–56.
7 Y. Shao, C. Wu, T. Wu, C. Yuan, S. Chen, T. Ding, X. Ye and Y. Hu, *Int. J. Biol. Macromol.*, 2018, **111**, 1281–1292.
8 P. T. K. M. Kumar, T. R. Mandlimath, P. Sangeetha, P. Sakthivel, S. K. Revathi, A. S. K. Kumar and S. K. Sahoo, *RSC Adv.*, 2015, 5108034–5108043.
9 R. Liu and A. Sen, *J. Am. Chem. Soc.*, 2012, **134**, 17505–17512.
10 W. Wei, Y. Dai, M. Guo and Y. Zhu, *J. Phys. Chem. C*, 2010, **114**, 10917–10921.
11 J. Tian, R. Liu, G. H. Wang, Y. Xu, X. F. Wang and H. G. Yu, *Appl. Surf. Sci.*, 2014, **319**, 324–331.
12 T. He and D. Wu, *J. Mater. Sci.: Mater. Electron.*, 2017, **10**, 7320–7325.
13 S. Zhao, Y. W. Zhang, Y. M. Zhou, K. B. Qiu, C. Zhang, J. S. Fang and X. L. Sheng, *J. Photochem. Photobiol., A*, 2018, **350**, 94–102.
14 Y. Chen, Q. Ma, H. Li, D. Wang, Q. D. Che, J. P. Wang, G. Wang and P. Yang, *J. Nanosci. Nanotechnol. Res.*, 2018, **18**, 2738–2745.
15 N. Durán, G. Nakazato and A. B. Seabra, *Appl. Microbiol. Biotechnol.*, 2016, **100**, 6555–6570.
16 S. R. Kabir, A. K. M Asaduzzaman, R. Amin, A. S. M. T. Haque, R. Ghose, Md. M. Rahman, J. Islam, Md. B. Amin, I. Hasan, T. Debnath, B.-S. Chun, X. D. Zhao, M. K. R. Khan and M. T. Alam, *ACS Omega*, 2020, **5**, 20599–20608.
17 X. Dong, X. Ji, H. Wu, L. Zhao, J. Li and W. Yang, *J. Phys. Chem. C*, 2009, **113**, 6573–6576.
18 A. Haider and I.-K. Kang, *Adv. Mater. Sci. Eng.*, 2015, 165257.
19 A. Maynard and E. S. Michelson, *The nanotechnology consumer products inventory*, Wilson International Center for Scholars, 2006.

20 M. Rai, A. Yadav and A. Gade, *Biotechnol. Adv.*, 2009, **27**, 76–83.

21 C. Marambio-Jones and E. M. V. Hoek, *J. Nanopart. Res.*, 2010, **12**, 1531–1551.

22 L. Dong, D. Liang and R. Gong, *Eur. J. Inorg. Chem.*, 2012, **2012**, 3200–3208.

23 S. Saez, C. Fasciani, K. G. Stamplecoskie, L. B.-P. Gagnon, T.-F. Mah, M. L. Marin, E. I. Alarcon and J. C. Scaiano, *Photochem. Photobiol. Sci.*, 2015, **14**, 661–664.

24 R. A. Khaydarov, R. R. Khaydarov, O. Gapurova, Y. Estrin and T. Scheper, *J. Nanopart. Res.*, 2009, **11**, 1193–1200.

25 K. Naghavi, E. Saion, K. Rezaee and W. M. M. Yunus, *Radiat. Phys. Chem.*, 2010, **79**, 1203–1208.

26 M. A. Faramarzi and A. Sadighi, *Adv. Colloid Interface Sci.*, 2013, **189**, 1–20.

27 S. Gurunathan, J. W. Han, E. S. Kim, J. H. Park and J. H. Kim, *Int. J. Nanomed.*, 2015, **10**, 2951–2969.

28 M. Valodkar, A. Badhoria, J. Pohnerkar, M. Mohan and S. Thakore, *Carbohydr. Res.*, 2010, **345**, 1767–1773.

29 G. F. Fanta, J. A. Kenar, F. C. Felker and J. A. Byars, *Carbohydr. Polym.*, 2013, **92**, 260–268.

30 M. Lavorgna, I. Attianese, G. Buonocore, A. Conte, M. del Nobile, F. Tescione and E. Amendola, *Carbohydr. Polym.*, 2014, **102**, 385–392.

31 Y. O. Kang, T. S. Lee and W. H. Park, *J. Mater. Sci.: Mater. Med.*, 2014, **25**, 2629–2638.

32 W. Hu, S. Chen, X. Li, S. Shi, W. Shen, X. Zhang and H. Wang, *Mater. Sci. Eng. C*, 2009, **29**, 1216–1219.

33 Y. W. Han and M. A. Clarke, *J. Agric. Food Chem.*, 1990, **38**, 393–396.

34 S. A. Kang, K.-H. Jang, J.-W. Seo, K. H. Kim, Y. H. Kim, D. Rairakhwada, *et al.*, *Microbial Production of Biopolymers and Polymer Precursors: Applications and Perspectives*, ed. B. Rehm, Caister Academic Press, Norwich, 2009.

35 S.-H. Yoo, E. J. Yoon, J. Cha and H. G. Lee, *Int. J. Biol. Macromol.*, 2004, **34**, 37–41.

36 R. Srikanth, C. H. Reddy, G. Siddartha, M. J. Ramaiah and K. B. Uppuluri, *Carbohydr. Polym.*, 2015, **120**, 102–114.

37 I. Dahech, B. Harrabi, K. Hamden, A. Feki, H. Mejdoub and K. S. Belghith, *Int. J. Biol. Macromol.*, 2013, **58**, 281–286.

38 S. Nakapong, R. Pichyangkura, K. Ito, M. Iizuka and P. Pongsawasdi, *Int. J. Biol. Macromol.*, 2013, **54**, 30–36.

39 I. Oktavia, A. N. Fithriah, N. U. Permatasari, E. Ratnaningsih and R. Hertadi, *Indian J. Chem.*, 2020, **20**, 493–502.

40 O. M. Bondarenko, A. Ivask, A. Kahru, H. Vija, T. Titma, M. Visnapuu, U. Joost, K. Pudova, S. Adamberg, T. Visnapuu and T. Alamäe, *Carbohydr. Polym.*, 2015, **136**, 710–720.

41 M. Taran, S. Etemadi and M. Safaei, *J. Appl. Polym. Sci.*, 2017, **134**, 44613.

42 A. Tabernero, Á. González-Garcinuño, J. M. SánchezÁlvarez, M. A. Galán and E. M. M. del Valle, *Carbohydr. Polym.*, 2017, **160**, 26–33.

43 F. Sima, E. C Mutlu, M. S. Eroglu, L. E. Sima, N. Serban, C. Ristoscu, S. M. Petrescu, E. T. Oner and I. N. Mihailescu, *Biomacromol*, 2011, **12**, 2251–2256.

44 A. Haddar, M. Hamed, A. Bouallegue, R. Bastos, E. Coelho and M. A. Coimbra, *Food Chem.*, 2021, **343**, 128456.

45 E. Renuart and C. Viney, *Pergamon Mater. Ser.*, 2000, 223–267.

46 K. B. A. Ahmed, D. Kalla, K. B. Uppuluri and V. Anbazhagan, *Carbohydr. Polym.*, 2014, **112**, 539–545.

47 Á. González-Garcinuño, R. Masa, M. Hernández, Á. Domínguez, A. Tabernero and E. del Valle, *Int. J. Mol. Sci.*, 2019, **20**, 1502.

48 M. Carbone, D. T. Donia, G. Sabbatella and R. Antiochia, *J. King Saud Univ., Sci.*, 2016, **28**, 273–279.

49 M. Jamal, W. Ahmad, S. Andleeb, F. Jalil, M. Imran, M. A. Nawaz, H. Tahir, A. Muhammadand, R. Muhammad and M. A. Kamil, *J. Chin. Med. Assoc.*, 2018, **81**, 7–11.

50 L. Segal, J. J. Creely, A. E. Martin and C. M. Conrad, *Text. Res. J.*, 1959, **29**, 786–794.

51 J. M. Andrews, *J. Antimicrob. Chemother.*, 2001, **48**, 5–16.

52 M. A. Ansari, H. M. Albetran, M. H. Alheshibri, A. Timoumi, N. A. Algarou, S. Akhtar, Y. Slimani, M. Almessiere, F. AlAhmari, A. Baykal, *et al.*, *Antibiotics*, 2020, **9**, 572.

53 U. Baig, M. A. Ansari, M. A. Gondal, S. Akhtar, F. A. Khan and W. S. Falath, *Mater. Sci. Eng. C*, 2020, **22**, 110992.

54 K. Iwata, S. Ishizaki, A. Handa and M. Tanaka, *Fish. Sci.*, 2000, **66**, 372–378.

55 W. Xu, Q. Liu, Y. Bai, S. Yu, T. Zhang, B. Jiang and W. Mu, *Int. J. Biol. Macromol.*, 2018, **109**, 810–818.

56 C. C. Luo, Y. H. Zhang, X. W. Zeng, Y. W. Zeng and Y. G. Wang, *J. Colloid Interface Sci.*, 2005, **288**, 444–448.

57 S. Boufi, M. R. Vilar, A. M. Ferraria and A. M. B. d. Rego, *Colloids Surf., A*, 2013, **439**, 151–158.

58 P. Kelter, M. Mosher and A. Scott, *Chemistry: The Practical Science*, Houghton Mifflin Company, Boston, 2009, ch. 9.

59 J. Zhang, X. Yue, Y. Zeng, E. Hua, M. Wang and Y. Sun, *Biotechnol. Biotechnol. Equip.*, 2018, **32**, 1583–1589.

60 K. Kawahara, K. Tsuruda, M. Morishita and M. Uchida, *Dent. Mater.*, 2000, **16**, 452–455.

61 A. Taglietti, Y. A. D. Fernández, E. Amato, L. Cucca, G. Dacamo, P. Grisoli, V. Necchi, P. Pallavicini, L. Pasotti and M. Patrini, *Langm*, 2012, **28**, 8140–8148.

62 K. Okaiyeto, M. O. Ojemaye, H. Hoppe, L. V. Mabinya and A. I. Okoh, *Molecules*, 2019, **24**, 4382.

63 M. Zhao, X. Hou, L. Lv, Y. Wang, C. Li and A. Meng, *Mater. Sci. Eng. C*, 2019, **98**, 83–88.

64 B. Hu, N. Wang, L. Han, M.-L. Chen and J.-H. Wang, *Acta Biomater.*, 2015, **11**, 511–519.

65 I. Sondi and B. Salopek-Sondi, *J. Colloid Interface Sci.*, 2004, **275**, 177–182.

66 M. Kowshik, S. Ashtaputre, S. Kharrazi, W. Vogel, J. Urban, S. K. Kulkarni and K. M. Paknikar, *Nanotechnology*, 2002, **14**, 95.

67 C. G. Kumar and P. Sujitha, *Nanotechnology*, 2014, **25**, 325101.

68 M. A. Ansari, H. M. Khan, A. A. Khan, S. S. Cameotra, Q. Saquib and J. Musarrat, *J. Basic Microbiol.*, 2014, **54**, 688–699.

69 V. Amutha, P. Deepak, C. Kamaraj, G. Balasubramani, D. Aiswarya, D. Arul, P. Santhanam, A. M. Ballamurugan and P. Perumal, *J. Cluster Sci.*, 2019, **30**, 797–812.

70 R. K. Dhall and M. S. Alam, *Encyclopedia of Renewable and Sustainable Materials*, Elsevier, 2020, pp. 26–43, ISBN 9780128131961.

71 S. Hajji, R. B. Salem, M. Hamdi, K. Jellouli, W. Ayadi, M. Nasri and S. Boufi, *Process Saf. Environ. Prot.*, 2017, **111**, 112–121.

72 S. Xin, L. Xiao, X. Dong, X. Li, Y. Wang, X. Hu, D. E. Sameen, W. Qin and B. Zhu, *Int. J. Biol. Macromol.*, 2020, **164**, 211–221.

73 W. G. Sganzerla, M. Longo, J. L. de Oliveira, C. G. da Rosa, A. P. de LimaVeeck, R. S. de Aquino, A. V. Masiero, F. C. Bertoldi, P. L. M. Barreto and M. R. Nunes, *Colloids Surf., A*, 2020, **602**, 125125.

74 Y. Li and Y. Ding, *J. Phys. Chem. C*, 2010, **114**, 3175–3179.

75 V. Falguera, J. P. Quintero, A. Jiménez, J. A. Muñoz and A. Ibarz, *Trends Food Sci. Technol.*, 2011, **22**, 292–303.

76 L. Angiolillo, A. Conte and M. A. Del Nobile, *Reference Module in Food Science*, Elsevier, 2016.

77 L. Atarés and A. Chiralt, *Trends Food Sci. Technol.*, 2016, **48**, 51–62.

78 JFHA: Japan Food Hygiene Association, *Standard methods of analysis in food safety regulation*, 2015.

79 Y. Xing, W. Li, Q. Wang, X. Li, Q. Xu, X. Guo, X. Liu, X. Bi, Y. Shui, H. Lin and H. Yang, *Molecules*, 2019, **24**, 1695.

80 X. He, H. Deng and H. Hwang, *J. Food Drug Anal.*, 2019, **27**, 1–21.

81 S. Kumar, A. Mukherjee and J. Dutta, *Trends Food Sci. Technol.*, 2020, **97**, 96–209.

82 European Commission Regulation, *European Commission Regulation (EU) No 10/2011 of 14 January 2011 on plastic materials and articles intended to come into contact with food*, 2011, https://eur-lex.europa.eu/legal-content/EN/TXT/?uri=CELEX:02011R0010-20190829.